

The matching of 3D Rolie-Poly viscoelastic numerical simulations with experimental polymer melt flow within a slit and a cross-slot geometry

T. D. Lord, L. Scelsi, D. G. Hassell,^{a)} and M. R. Mackley^{b)}

Department of Chemical Engineering, University of Cambridge, Pembroke Street, Cambridge CB2 3RA, United Kingdom

J. Embery and D. Auhl

IRC in Polymer Science and Technology, Department of Physics and Astronomy, University of Leeds, Leeds LS2 9JT, United Kingdom

O. G. Harlen

School of Mathematics, University of Leeds, Leeds LS2 9JT, United Kingdom

R. Tenchev,^{c)} P. K. Jimack, and M. A. Walkley

School of Computing, University of Leeds, Leeds LS2 9JT, United Kingdom

(Received 22 July 2009; final revision received 22 December 2009; published 9 March 2010)

Synopsis

This paper is concerned with matching a fully three-dimensional (3D) viscoelastic numerical simulation with experimental results obtained using a multi-pass rheometer for both an entry-exit slit flow and a cross-slot geometry. The 3D code simulates the time evolution of steady flows using a multi-mode Rolie-Poly constitutive equation. A test polydisperse polystyrene was characterized for both its linear and non-linear viscoelastic response and the rheological parameters were used for the simulation with matching boundary conditions for the flow. Both overall pressure difference and flow birefringence were compared for the entry-exit slit flow and good matching between simulation and experiment was found for the three different depth geometries tested. The 10 mm depth results (depth to width aspect ratio of 6.7:1) also showed that a 2D simulation gave a close match to both 3D simulation and experimental results. The flow birefringence fit between experiment and simulation for the cross-slot case, while reasonable, did not match as well as the slit and the results demonstrate that the cross-slot geometry is very sensitive to the extensional behavior of the melt. In addition, examples of the application of the 3D code are given for a monodisperse polystyrene, where the match to experiment proved as good as that of the test polydisperse polystyrene. © 2010 The Society of Rheology. [DOI: 10.1122/1.3306572]

^{a)}Present address: Department of Chemical Engineering, University of Nottingham Malaysia Campus, Jalan Broga, 43500 Semenyih, Selangor D.E., Malaysia.

^{b)}Author to whom all correspondence should be addressed; electronic mail: mrm5@cam.ac.uk

^{c)}Present address: LUSAS, Forge House, 66 High Street, Kingston upon Thames, Surrey KT1 1HN, United Kingdom.

I. INTRODUCTION

The modeling of viscoelastic flow within complex flow geometries has now developed to an extent where it is realistic to simulate the flow behavior of commercial viscoelastic polymer melts. Numerical simulation techniques have steadily advanced over the last three decades [see, for example, Keunings (1989); Baaijens (1998); Phillips and Owens (2002); Clemeur *et al.* (2004); Binding *et al.* (2006); Alves *et al.* (2008); Puangkird *et al.* (2009)]. Experimental methods for characterizing both linear and non-linear viscoelastic rheology for commercial polymers have also advanced to a stage where multi-parameter descriptions are possible [Mackley *et al.* (1994); Inkson *et al.* (1999); Friedrich *et al.* (2008); Reptate¹ and IRIS Rheo-Hub²].

A variety of different forms of constitutive equation have been proposed to describe molten polymer viscoelasticity, including differential models such as PTT [Phan-Thien and Tanner (1977)], integral constitutive equations of K-BKZ type [Wagner and Laun (1978); Wagner *et al.* (2008)], and tube theory based models such as the pom-pom [McLeish and Larson (1998)] and the Rolie-Poly model [Likhman and Graham (2003)]. Each of these constitutive equations has their various merits, however, in this paper, matching simulation with experiment is carried out exclusively using the Rolie-Poly constitutive equation. This model is appropriate for entangled linear polymers and incorporates the processes of reptation, chain retraction, and convective constraint release.

There are now a variety of different numerical solvers available for simulating viscoelastic flow based on finite element or finite volume methods, including commercial packages such as ANSYS POLYFLOW³ and REM3D,⁴ as well as codes developed by academic groups [see, for example, Bogaerds *et al.* (1999); Wapperom and Webster (1999); Oliveira *et al.* (1998); Luo and Mitsoulis (1990); Hulsen *et al.* (2001); Rasmussen (2002); Inkson *et al.* (2009)].

The development of constitutive equations, characterization, and numerical simulations is now at a stage where it is possible to carry out full three-dimensional (3D) transient simulations of the flow of a viscoelastic polymer melt. The main objective of this paper is to compare such a simulation to experiment for two well defined flows.

The two geometries chosen are an entry-exit slit [Lee *et al.* (2001); Hassell *et al.* (2009)] and a cross-slot flow [Verbeeten *et al.* (2002); Coventry and Mackley (2008); Soulages *et al.* (2008)]. These provide representative and challenging flow situations for both experiment and simulation. The flow geometries have been incorporated into the design of a double piston multi-pass rheometer (MPR) [Mackley *et al.* (1995)] which provides a platform for carrying out precise flow birefringence experiments for slit and cross-slot geometries of different depths.

A new 3D numerical solver “EUFLOW” [Tenchev *et al.* (2008)] is evaluated using rheological data for a particular polystyrene melt fitted to provide Rolie-Poly constitutive parameters. The simulation is then matched to a systematic set of different depth experimental data obtained using the MPR in order that a direct comparison can be made between simulation and experiment.

¹www.reptate.com

²<http://rheology.tripod.com>

³<http://www.ansys.com/products/polyflow>

⁴http://www.transvalor.com/rem3d_gb.php

II. MODELING AND EXPERIMENTAL METHODS

A. Constitutive equation and material characterization

1. The Rolie-Poly model

The Rolie-Poly model [Likhman and Graham (2003)] is a recent tube theory based model which incorporates the molecular motion mechanisms of reptation, contour-length fluctuations, and constraint release. It was developed in order to describe linear entangled polymers and is a simplified version of the Graham–Likhman–Milner–McLeish (GLaMM) model [Graham *et al.* (2003)]. In the multimode form of the Rolie-Poly model, the polymer stress \mathbf{T} is given by

$$\mathbf{T} = \sum g_i \boldsymbol{\sigma}_i, \quad (1)$$

where g_i is the relaxation modulus for mode i and $\boldsymbol{\sigma}_i$ is a dimensionless variable that satisfies

$$\begin{aligned} \frac{\partial \sigma_{jk}}{\partial t} + u_l \frac{\partial \sigma_{jk}}{\partial x_l} &= \frac{\partial u_j}{\partial x_l} \sigma_{lk} + \sigma_{jl} \frac{\partial u_k}{\partial x_l} - \frac{1}{\tau} (\sigma_{jk} - \delta_{jk}) \\ &\quad - \frac{2}{\tau_R} \left(1 - \sqrt{\frac{3}{\sigma_{ll}}} \right) \left(\sigma_{jk} + \beta \left(\frac{\sigma_{ll}}{3} \right)^\delta (\sigma_{jk} - \delta_{jk}) \right). \end{aligned} \quad (2)$$

Here, $\mathbf{u}(\mathbf{x}, t)$ is the fluid velocity and j, k, l are the standard Cartesian components with summation convention applied. The mode index, i , is suppressed for clarity. Each mode has two characteristic relaxation times: τ , the linear relaxation time governed by reptation for the relaxation of orientation and τ_R , the tube Rouse time associated with the relaxation of chain stretch. In addition, there are two more parameters, β and δ , that are concerned with convective constrain release (CCR). However, in this paper, we will take $\beta=0$ so that CCR is suppressed.

2. Material characterization

The test material used in this paper is a polydisperse commercial polystyrene (PS2), supplied by BASF SE. The molecular-weight distribution and polydispersity index M_w/M_n were determined using a triple detection size-exclusion chromatography apparatus (Viscotek TDA302) equipped with two PolymerLabs Mixed C columns running at 30 °C in tetrahydrofuran (Table I).

The polystyrene sample was characterized in both simple shear and uniaxial extensional flow at temperatures between 120 °C and 220 °C under a nitrogen atmosphere in order to prevent degradation. Shear flow experiments were conducted using an advanced rheometric expansion system (ARES) rheometer (Rheometric Scientific) in order to obtain the linear rheological and non-linear shear flow behaviors as well as the corresponding spectra. The non-linear elongational flow behavior was characterized using the uniaxial stretching device sentmanat elongational rheometer (Xpansion Instruments) attached to the ARES rheometer. The time-temperature superposition technique [Ferry

TABLE I. Table of molecular weight averages and polydispersity for PS2.

Label	M_w (kg/mol)	M_n (kg/mol)	M_w/M_n
PS2	273	101	2.7

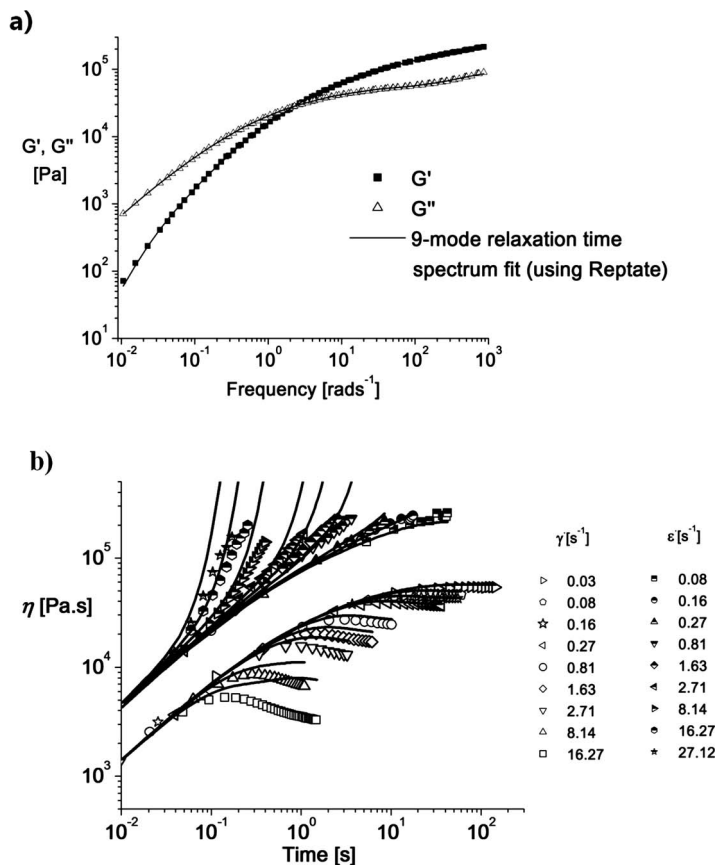


FIG. 1. Rheological data for PS2 at a reference temperature of 180 °C. (a) Linear visco-elastic shear storage and loss moduli G' and G'' fitted with a nine-mode Maxwell spectrum. (b) Non-linear shear and uniaxial extensional transient viscosities η (symbols) with corresponding Rolie-Poly model fits (solid lines).

(1980); Auhl *et al.* (2008)] was used to shift the experimental data to a reference temperature of 180 °C in order to obtain a master-curve and corresponding set of model parameters.

Figure 1(a) shows the complex modulus data with a time-temperature superposition and Fig. 1(b) shows the non-linear rheological data in shear and elongation and Rolie-Polie model fits. Table II lists the resulting model parameters obtained. A nine-mode Rolie-Poly parameter set was fitted to the elongational and non-linear shear flow data using the Reptate software package⁵ developed by Ramirez and Likhtman as part of the “Microscale Polymer Processing 2” project.⁶ A choice of nine modes was considered somewhat arbitrary, but considered adequate to capture the rheology as shown in Fig. 1. The model fit for this material is based on the relaxation time spectrum as determined in Fig. 1(a) and involves a distribution of molecular stretch times τ_R which captures the mild polydispersity of the sample. When appropriate stretch times are assigned to the modes of the distribution (cf. Table II), the parameters describe well the extension hardening as

⁵www.reptate.com

⁶www.mupp2.co.uk

TABLE II. Relaxation time spectrum and the corresponding non-linear constitutive parameters of the multi-mode Rolie-Poly model for PS2 at 180 °C.

PS2			
Mode No.	g_i (Pa)	τ_i (s)	τ_{Ri} (s)
1	1.421×10^5	4.500×10^{-4}	–
2	6.217×10^4	1.770×10^{-3}	–
3	4.409×10^4	7.030×10^{-3}	–
4	4.784×10^4	2.796×10^{-2}	–
5	3.772×10^4	1.111×10^{-1}	–
6	2.475×10^4	4.418×10^{-1}	0.1
7	1.084×10^4	1.756×10^0	1.0
8	2.535×10^3	6.982×10^0	3.0
9	5.250×10^2	2.775×10^1	6.0

well as the shear viscosity overshoots of the polydisperse polystyrene. In the case of modes 1–5, the Rouse relaxation time is short compared to the flow time scales and so for these modes, Eq. (2) is replaced by the non-stretching version of the Rolie-Poly model

$$\frac{\partial \sigma_{jk}}{\partial t} + u_l \frac{\partial \sigma_{jk}}{\partial x_l} = \frac{\partial u_j}{\partial x_l} \sigma_{lk} + \sigma_{jl} \frac{\partial u_k}{\partial x_l} - \frac{1}{\tau} (\sigma_{jk} - \delta_{jk}) - \frac{2}{3} \left(\sigma_{lm} \frac{\partial u_m}{\partial x_l} \right) (\sigma_{jk} + \beta (\sigma_{jk} - \delta_{jk})). \quad (3)$$

B. Numerical simulation

A Lagrangian finite element simulation technique [Harlen *et al.* (1995)], called *FLOW-SOLVE*, has been used in the past to predict the complex flow behavior observed in the MPR [see, for example, Lee *et al.* (2001); Collis *et al.* (2005); Hassell *et al.* (2008)]. This code is currently restricted to two-dimensional (2D) planar and axisymmetric flows. A finite element simulation is used in this paper, referred to here as “*EUFLOW*” [Tenchev *et al.* (2008)], as this is able to simulate the fully 3D flow within the MPR. For the MPR simulations used in this paper, a fixed finite element grid is used, although *EUFLOW* can also model small boundary and free surface deformations using the arbitrary Lagrangian Eulerian framework [Walkley *et al.* (2005)].

It is assumed that both inertia and compressibility effects are negligible due to the fluid viscosity, and size and flow-rates within the MPR, so that the momentum and mass conservation equations reduce to

$$\nabla \cdot \mathbf{T} - \nabla p = 0, \quad (4)$$

$$\nabla \cdot \mathbf{u} = 0, \quad (5)$$

where p is the pressure and \mathbf{T} is the stress defined in Eq. (1). The spectrum of modes is divided into two groups in the method described by Collis *et al.* (2005). We define fast relaxing modes as modes where $\dot{\gamma}_w \tau_i \ll 0.01$ (where $\dot{\gamma}_w$ is the wall shear rate), which are treated as a Newtonian solvent. The remaining slower modes are treated explicitly, thus

$$\mathbf{T} = \mu (\nabla \mathbf{u} + (\nabla \mathbf{u})^T) + \sum_{\text{slow}} g_i \boldsymbol{\sigma}_i, \quad (6)$$

where $\mu = \sum_{\text{fast}} g_i \tau_i$ is the effective Newtonian viscosity.

Since the Stokes equations (4) and (5) are independent of time, the only explicitly time-dependent equations are the evolution equations for the polymer stress (2). Thus we can separate the solution of the Stokes equations from the constitutive equation by solving the fluid velocity \mathbf{u} using the current values of the $\boldsymbol{\sigma}_i$ and then updating $\boldsymbol{\sigma}_i$ by time stepping Eq. (2) using the following scheme:

$$\frac{1}{\Delta t} \sigma_{jk}^{n+1} + u_l^n \frac{\partial \sigma_{jk}^{n+1}}{\partial x_l} - \sigma_{jl}^{n+1} \frac{\partial u_k^n}{\partial x_l} - \sigma_{lk}^{n+1} \frac{\partial u_j^n}{\partial x_l} + \frac{\sigma_{jk}^{n+1}}{\tau_\sigma^n} = \frac{1}{\Delta t} \sigma_{jk}^n + \frac{\delta_{jk}}{\tau_\delta^n}, \tag{7}$$

where

$$\frac{1}{\tau_\delta^n} = \frac{1}{\tau} + \frac{2}{\tau_R} \beta \left(\frac{\sigma_{ll}^n}{3} \right)^\delta \left(1 - \sqrt{\frac{3}{\sigma_{ll}^n}} \right), \tag{8a}$$

$$\frac{1}{\tau_\sigma^n} = \frac{1}{\tau_\sigma^n} + \frac{1}{\tau_R}. \tag{8b}$$

Note that in the case $\beta=0$, the relaxation times τ_σ^n and τ_δ^n become time and space independent. For the hyperbolic system equation (7), a standard Galerkin finite element discretization leads to numerical solutions in which non-physical oscillations are observed. These are removed through the use of streamline upwind Petrov–Galerkin (SUPG). Two upwinding schemes have been implemented: full SUPG using the implementation of Fan *et al.* (1999) and what is referred in this paper as “selective upwinding” [Yu and Heinrich (1987)], in which upwinding is only applied to the test function multiplying the advection term in Eq. (7). Little difference is found in the results of the two different schemes, however, selective upwinding gives slightly smoother predictions for the stress fields and was used for the results presented in this paper. The resulting system of linear equations is solved iteratively using BiCGStab with an ILU preconditioner [Saad (2003)].

The fluid velocity \mathbf{u} is obtained from the solution of the Stokes equations (4) and (5) with the stress contribution from the “slow” modes treated as a known forcing term. To eliminate the pressure, we use a penalty formulation in which the incompressibility constraint equation (5) is replaced by

$$\nabla \cdot \mathbf{u} = -\frac{1}{\chi} p. \tag{9}$$

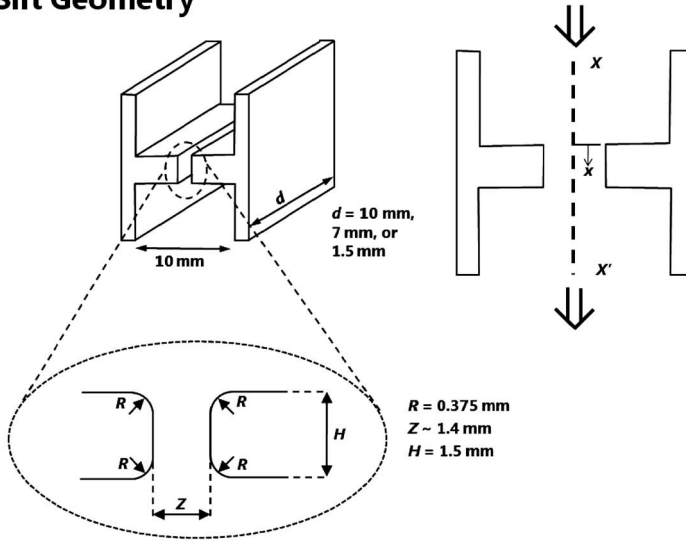
Provided the value of the penalty parameter χ is chosen to be sufficiently large, the incompressibility condition is recovered. Furthermore, in practice, no fluid is truly incompressible and the value of χ used is larger than the actual bulk modulus of the material. Substituting Eqs. (6) and (9) into Eq. (4) and noting that $\chi \gg \mu$, the momentum equation becomes

$$-\nabla \cdot (\mu \nabla \mathbf{u}) - \nabla(\chi \nabla \cdot \mathbf{u}) = \nabla \cdot \left(\sum_{\text{slow}} g_i \boldsymbol{\sigma}_i \right). \tag{10}$$

This is discretized using either quadrilateral (2D) or hexahedral finite elements using the standard Galerkin approximation. Since the left-hand side operator remains fixed in time, the matrix of the resulting linear system remains constant throughout the simulation. Consequently, this matrix only needs to be factorized once and so we have developed our own direct out-of-core LU factorization to allow large 3D problems to be solved.

In order to validate this simulation method, 2D planar simulations were compared to results obtained with the Lagrangian finite element method [Harlen *et al.* (1995)] for a entry-exit flow geometry, a 2D version of Fig. 2(a). These two methods use quite differ-

a) Slit Geometry



b) Cross-slot Geometry

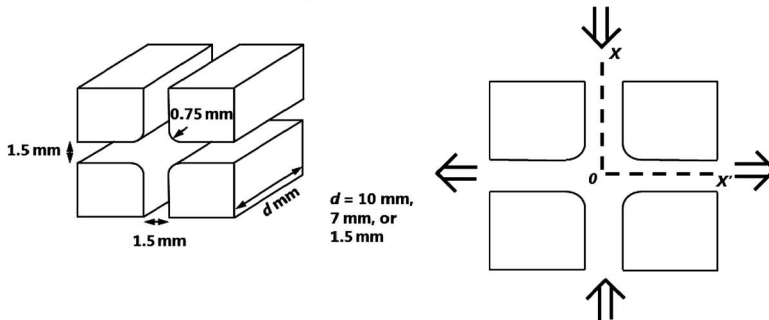


FIG. 2. The experimental MPR slit geometries. (a) Experimental MPR entry-exit slit geometry. LHS geometry dimensions, right-hand side (RHS) schematic showing flow direction and center-line profile $X-X'$. (b) MPR cross-slot geometry. LHS geometry dimensions, RHS schematic showing flow direction. The profile $X-O-X'$ is used as the center-line profile.

ent approximations for both the velocity and constitutive equation. Figures 3(a)–3(c) show a comparison of the flow birefringence, pressure drop, and principal stress difference (PSD) along the center line for flow conditions equivalent to an upstream mean flow velocity of 0.3 mm s^{-1} in a 10 mm depth channel. The results show a clear match.

In order to assess whether the *EUFLOW* grid used gave a convergence of the solution, the same simulation was conducted using a grid two times finer and a grid two times coarser. The results show that the same solution is achieved with each grid, indicating convergence. Thus the grid used is sound. The results comparing the PSD for each grid are shown in Fig. 3(d). A more complete description of the *EUFLOW* software, along with further validation results, may be found in [Tenchev *et al.* \(2008\)](#).

C. The MPR: Geometries and experimental protocol

The MPR is a dual piston rheometer, consisting of two servo-hydraulically driven pistons that can be moved separately or together, allowing a wide range of rheological

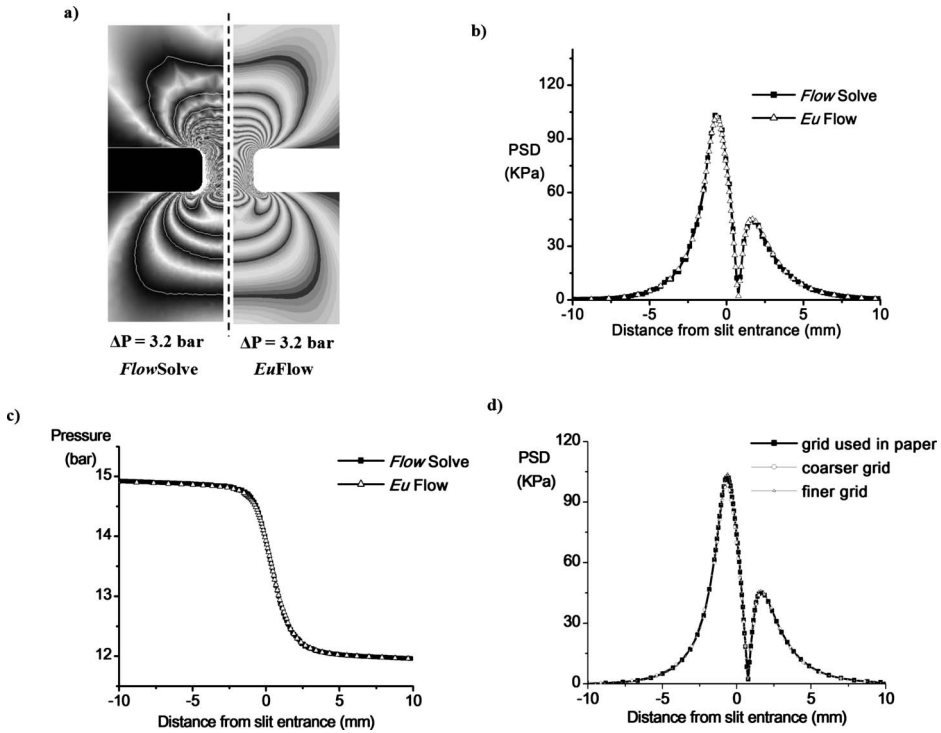


FIG. 3. Comparison of 2D *EUFLOW* with 2D *FLOWSOLVE* simulations. (a) Comparison of PSD contours and overall pressure drop for *FLOWSOLVE* and *EUFLOW*. MPR slit flow $\bar{u}=0.3$ mm s⁻¹ for notional 10 mm depth. (b) Center-line PSD as a function of distance along center-line. (c) Center-line pressure as a function of distance along center-line. (d) Results of center-line PSD as a function of distance along center-line for different simulation grids.

deformations to be imposed on the fluid contained within an enclosed volume. Pressure transducers on either side of the central test section enable pressure measurements to be made. The central test section is designed such that flow through different geometries (determined by the insert used) can be observed optically. The basic concept of the MPR is described in detail by Mackley *et al.* (1995) and with the use of the optical cell described by Lee *et al.* (2001).

Two different geometries, an entry-exit slit and a cross-slot, were used in this work. These geometries are shown in Fig. 2. The entry-exit slit geometry [Hassell *et al.* (2009)] has rounded inlet and outlet corners to improve both experimental observations and numerical simulations. The entry-exit slit geometry creates regions of high simple shear near to the slit walls and extensional flow in the region of the symmetry line in the inlet and outlet areas of the flow. The cross-slot geometry was developed for the MPR by Coventry and Mackley (2008). This flow configuration creates a pure extensional flow deformation in the central region about the stagnation point of the flow, together with essentially simple shear near the outer curved walls. The operation of the MPR using these two geometries has been described elsewhere, for both the entry-exit slit [Collis and Mackley (2005)] and the cross-slot [Coventry and Mackley (2008)]. In order to explore 3D effects of the flow, the geometries used each had depths of 1.5, 7, and 10 mm, with channel width of 1.5 mm. These gave depth to width aspect ratios of $\approx 1:1$, 4.7:1, and 6.7:1.

D. Flow induced birefringence

Flow induced birefringence was used to observe the PSD during flow. Monochromatic polarized light with a wavelength of 514 nm was passed through the midsection and orthogonal analyzer before being captured using a digital video camera. Quarter wave plates were used to eliminate the isoclinic extinction bands to leave only the stress-related isochromatic fringes.

All flow experiments were carried out at 180 °C and a stress optical coefficient value of $-4 \times 10^{-9} \text{ Pa}^{-1}$ was used, in line with the value used in previous studies on polystyrene [Macosko (1994); Han and Dexler (1973); Collis and Mackley (2005)]. As discussed by Clemeur *et al.* (2004), in order to calculate the position of the isochromatic fringes in a 3D flow, it is necessary to integrate over the light path through the sample. This calculation can be performed using Mueller calculus [Fuller (1995)], in which each component of the optical train is represented by a 4×4 Mueller matrix, \mathbf{M} . For the experiment described above, the light intensity I_f at the detector is related to the transmitted intensity I by

$$I_f = \frac{I}{4}(M_{11} - M_{44}), \quad (11)$$

where M_{ij} is the ij component of the Mueller matrix of the flow cell. For transmission along the z -axis, \mathbf{M} is found by integrating the equation [Clemeur *et al.* (2004)]

$$\frac{d\mathbf{M}(z)}{dz} = \mathbf{m}(z)\mathbf{M}(z), \quad (12)$$

with $\mathbf{M}=\mathbf{I}_4$ at $z=0$, where $\mathbf{m}(z)$ is given by

$$\mathbf{m}(z) = \frac{2\pi C}{\lambda} \begin{pmatrix} 0 & 0 & 0 & 0 \\ 0 & 0 & 0 & -2T_{xy} \\ 0 & 0 & 0 & (T_{xx} - T_{yy}) \\ 0 & 2T_{xy} & -(T_{xx} - T_{yy}) & 0 \end{pmatrix}. \quad (13)$$

Here, C is the stress optical coefficient and λ is the wavelength of light used. This integration is done in a post-processing step.

III. RESULTS AND DISCUSSION

A. Slit flow simulations and experiment comparisons

In this section, experimental MPR steady state results and the corresponding multi-mode Rolie-Poly simulations are presented for the 10, 7, and 1.5 mm depth slit flows. An illustration of the grid used for simulations is shown in Fig. 4(a).

For the 10 mm depth slit flow, a MPR experiment was performed with an upstream mean flow velocity, \bar{v} , of 0.06 mm s^{-1} , and both 2D and fully 3D numerical simulations corresponding to this experiment were carried out. Figure 5(a) compares the 2D and 3D simulations and demonstrates that at this depth the 2D approximation matches well with the full 3D flow both in terms of the pressure drop and PSD profiles. The 2D simulation gives a 9% lower pressure drop compared to the 3D simulation since it does not take into account the presence of the viewing window walls.

An example of the 3D *EUFLOW* simulation ranked against the steady state MPR experiment data is shown in Fig. 5(b) and here there is a very good match to the pressure difference measurements, the center line PSD profiles, and the overall PSD contour pattern. For Fig. 5(b), the apparent wall shear rate, $\dot{\gamma}_w$, was of order 1.9 s^{-1} , which, for

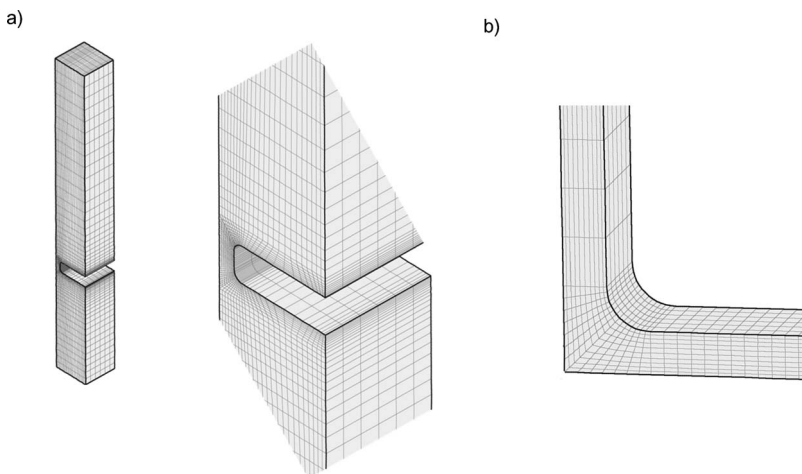


FIG. 4. 3D *EUFLOW* finite element grids used for the 3D simulations. (a) Entry-exit slit, with a close up view of the entry-exit region. (b) Cross-slot grid.

a mean linear relaxation time, $\bar{\tau} = \sum_{i=1}^n \tau_i / n$ (where n is total number of modes), of 4.1 s, gives a Weissenberg number, \bar{Wi} , of 7.8. The Weissenberg number for the longest linear relaxation time, Wi_m , would correspond to 52.7.

A second higher upstream mean flow velocity of 0.35 mm s^{-1} ($\dot{\gamma}_w \sim 10.6 \text{ s}^{-1}$) was also investigated for the 10 mm depth slit flow and the steady state MPR experiment and corresponding 3D *EUFLOW* simulation results are displayed in Fig. 5(c). At this higher flow rate, again a very good agreement between simulation and experiment was also achieved for both pressure drop and PSD profiles. For the situation in Fig. 5(c), \bar{Wi} and Wi_m were 43.5 and 294.2 respectively. For this flow rate, the time evolution of both the MPR experiment and the 3D *EUFLOW* simulation progression was also recorded and is shown in Fig. 6. Transient stress fangs [Lee *et al.* (2001)] are observed in the MPR experiment in the exit region of the flow and these features are also seen in the simulation showing that the Rolie-Poly constitutive equation can predict stress fangs for this particular set of flow conditions and this particular polymer. The overall PSD contours evolution is captured reasonably well, together with a good match of the stress fang evolution and this indicates that the multi-mode Rolie-Poly is a valid constitutive equation to describe the flow behavior of the polydisperse linear polymer within this complex flow situation.

In order to capture the 3D effect of depth, where the “front and back” glass observation faces influence the birefringence pattern, flow in a 7 and a 1.5 mm depth slit was investigated. For the 7 mm depth slit, an MPR experiment was conducted using $\bar{v} = 0.35 \text{ mm s}^{-1}$ (giving $\dot{\gamma}_w \sim 10.6 \text{ s}^{-1}$, $\bar{Wi} = 43.5$, and $Wi_m = 294.2$) and the corresponding 3D *EUFLOW* simulation was performed [Fig. 7(a)]. Again, good agreement is achieved for both pressure differences, PSD profiles and PSD contours.

For the case of the 1.5 mm depth slit, genuinely 3D flow is produced with the slit width and depth nearly the same. An MPR experiment was conducted with an $\bar{v} = 0.33 \text{ mm s}^{-1}$ (giving $\dot{\gamma}_w \sim 11.2 \text{ s}^{-1}$, $\bar{Wi} = 45.9$, and $Wi_m = 310.8$) together with the corresponding 3D *EUFLOW* simulation. The results are compared in Fig. 7(b). While the match is not excellent, the form of the flow birefringence pattern is very different to that observed in the 10 mm depth slit and the simulation captures most of the experimental

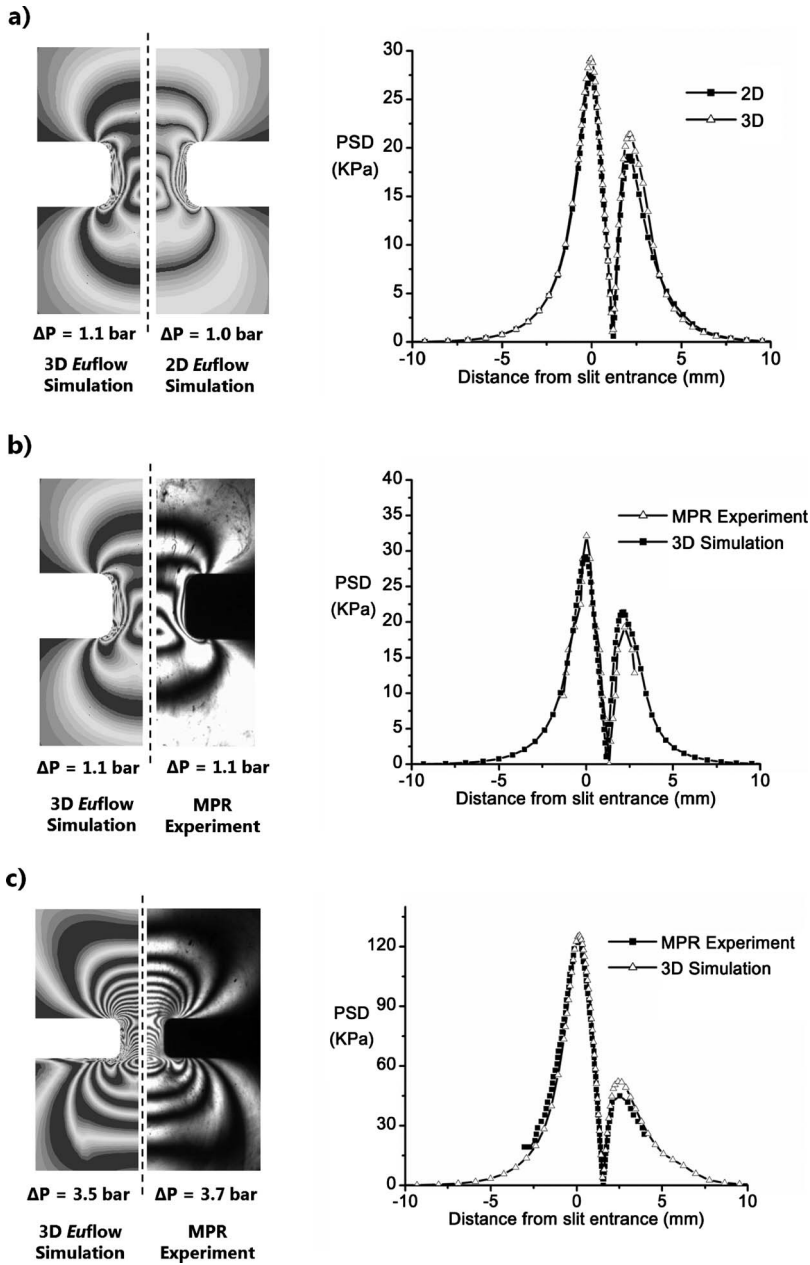


FIG. 5. Slit flow PSD contours, center-line PSD, and overall pressure drop for 10 mm depth. (a) Comparison between 3D and 2D *EUFLOW* simulations for $\bar{v}=0.06$ mm s⁻¹. (b) 3D *EUFLOW* comparison to experimental MPR flow for $\bar{v}=0.06$ mm s⁻¹, $\dot{\gamma}_w \sim 1.9$ s⁻¹, $\bar{W}i=7.8$ m and $Wi_m=52.7$. (c) 3D *EUFLOW* comparison to experimental MPR flow for $\bar{v}=0.35$ mm s⁻¹, $\dot{\gamma}_w \sim 10.6$ s⁻¹, $\bar{W}i=43.5$, and $Wi_m=294.2$.

features reasonably well. For this situation, the entry flow simulation grid shown schematically in Fig. 4(a) was unrealistic as the experimental upstream aspect ratio did not continue in the way modeled. The simulation pressure difference that has been recorded corresponds to the simulated pressure difference over a distance 5 mm upstream and

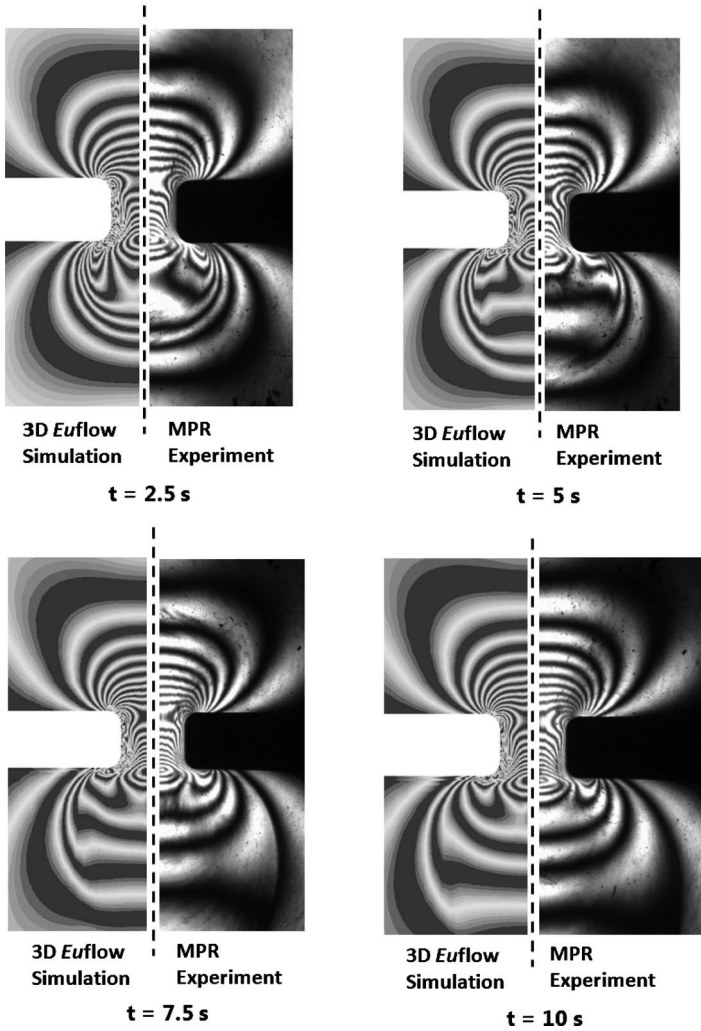


FIG. 6. 10 mm depth slit flow time evolution of PSD contours from rest for an MPR slit flow with $\bar{v} = 0.35 \text{ mm s}^{-1}$. For each time step, LHS is *EUFLOW* 3D simulation and RHS is experimental MPR flow.

downstream of the slit section where 5 mm is the experimental distance before the experimental flow channel opens out and changes dimension at the glass window extremity.

B. Cross-slot simulations and experiment comparisons

In this section, MPR experiments and corresponding multi-mode Rolie-Poly *EUFLOW* simulations were conducted for 10, 7, and 1.5 mm depth cross-slot geometries. The cross-slot grid used is shown in Fig. 4(b). Cross-slot simulations were found to be more challenging compared to the entry-exit slit flow, even at a 10 mm depth presumably due to the richness of the extensional strain history in the central region of the cross-slot. In the central region of the flow, infinite extensional strains exists [Crowley *et al.* (1976)]. Pressure drop data are not reported because experimentally most of the pressure drops

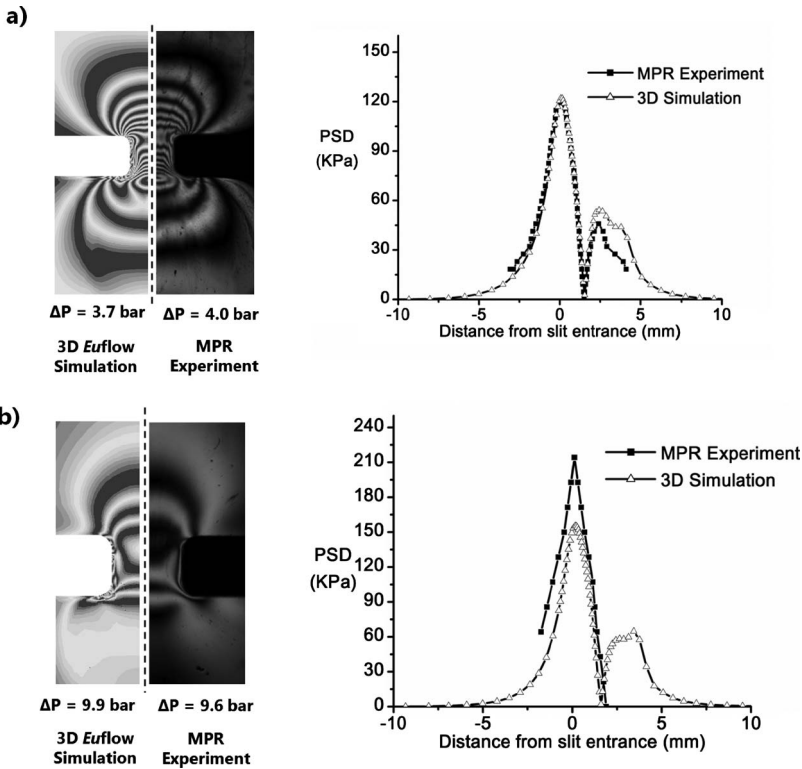


FIG. 7. The effect of slit depth. 3D *EUFLOW* simulations and experimental MPR PSD contours, center-line PSD, and overall pressure drop for (a) 7 mm depth slit ($\bar{v}=0.35$ mm s⁻¹, $\dot{\gamma}_w \sim 10.6$ s⁻¹, $\bar{Wi}=43.5$, and $Wi_m=294.2$) and (b) 1.5 mm depth slit ($\bar{v}=0.33$ mm s⁻¹, $\dot{\gamma}_w \sim 11.2$ s⁻¹, $\bar{Wi}=45.9$, and $Wi_m=310.8$).

originate from the side walls of the cross-slot flow and the entry and exit of the cross-slot device.

For the 10 mm depth cross-slot case, an MPR experiment was conducted with $\bar{v} = 2.3$ mm s⁻¹ (giving $\dot{\gamma}_w \sim 10.6$ s⁻¹, $\bar{Wi}=43.4$, and $Wi_m=294.2$) and a corresponding *EUFLOW* simulation was performed, with the time evolution recorded. The results are given in Fig. 8 and the simulation matches the experiment reasonably well for the time evolution and captures the cusping of the birefringence fringes along the center-line. The simulation features near the central region of the flow are problematic to resolve where the extensional strain becomes very high. The Rolie-Poly model used did not contain a limiting finite extensibility term and this may be the origin of the difficulty. However, the overall contour shapes match reasonably well.

As with the entry-exit slit, the effect of depth was explored by conducting an experiment and simulation at 7 mm depth and 1.5 mm depth, respectively. For the 7 mm depth cross-slot geometry, $\bar{v}=0.45$ mm s⁻¹ was used (giving $\dot{\gamma}_w \sim 2.1$ s⁻¹, $\bar{Wi}=8.4$, and $Wi_m=57.2$). The results comparing the *EUFLOW* simulation and the approximate steady state MPR experiment result are displayed in Fig. 9(a). The match is reasonable, with the discrepancy possibly associated with the high strain created in the central cross-slot region.

A fully 3D flow was examined using a 1.5 mm depth slit and the results between experiment and simulation are shown in Fig. 9(b) for $\bar{v}=2.44$ mm s⁻¹, which gave $\dot{\gamma}_w$

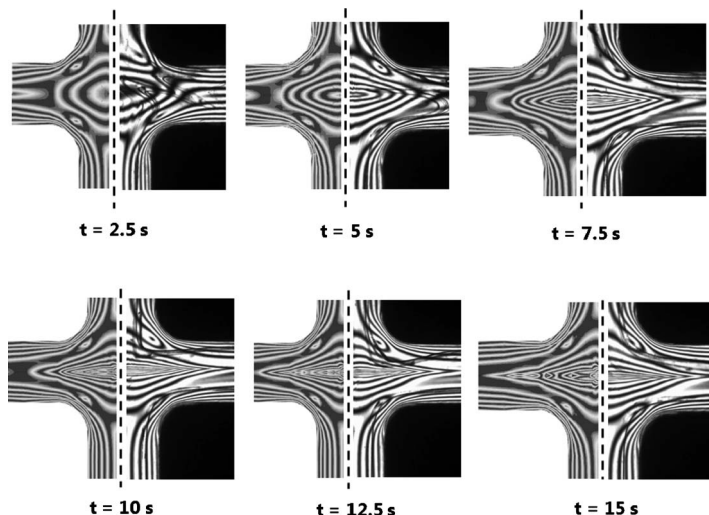


FIG. 8. Time evolution of PSD contours from rest for 10 mm depth cross-slot flow. MPR $\bar{v}=2.3 \text{ mm s}^{-1}$, $\dot{\gamma}_w \sim 10.6 \text{ s}^{-1}$, $\bar{Wi}=43.4$, and $Wi_m=294.2$. For each time step, LHS is *EUFLOW* 3D simulation and RHS is experimental MPR flow.

$\sim 11.2 \text{ s}^{-1}$, $\bar{Wi}=45.9$, and $Wi_m=310.8$. The simulation proved very challenging, with the 3D simulation providing only a remote match with the MPR experiment. When the cross-slot depth is large, as, for example, in Fig. 8, the birefringence pattern has characteristic features relating to the wall stress near the edges of the flow and also a characteristic central extensional flow stress region. When the flow is fully 3D, as in Fig. 9(b), these features are lost and both the experimental and simulated birefringence patterns become more difficult to interpret.

C. Monodisperse simulations and experiment comparisons

Monodisperse materials have in the past proved useful model systems to provide benchmark experiments for comparison to theory because of their precisely controlled molecular architecture [see, for example, Collis *et al.* (2005)]. These materials are only available in limited quantities and while their behavior is less complex than polydisperse materials [see, for example, Collis and Mackley (2005); Hassell and Mackley (2009)], the small amount of sample that is required for the MPR allows for comparison to predictive modeling.

In order to assess the ability of the *EUFLOW* code and the Rolie-Poly constitutive equation to simulate these model materials, a monodisperse polystyrene (DOW1568) was considered, which has been used in a number of recent melt flow studies [Hassell *et al.* (2009); Hassell and Mackley (2009)]. The material was characterized using gel permeation chromatography (GPC) with the method described in Sec. II and the properties listed in Table III.

The monodisperse polymer was characterized in both simple shear and uniaxial extensional flow in the same way as the PS2 material (detailed in Sec. II). A five-mode Rolie-Poly parameter set was fitted to the rheological data using *REPTATE* with the same methods as was used to characterize the PS2 material described in Sec. II. The fitted parameters are listed in Table IV.

An entry-exit MPR experiment was conducted using $\bar{v}=0.78 \text{ mm s}^{-1}$, giving $\dot{\gamma}_w$

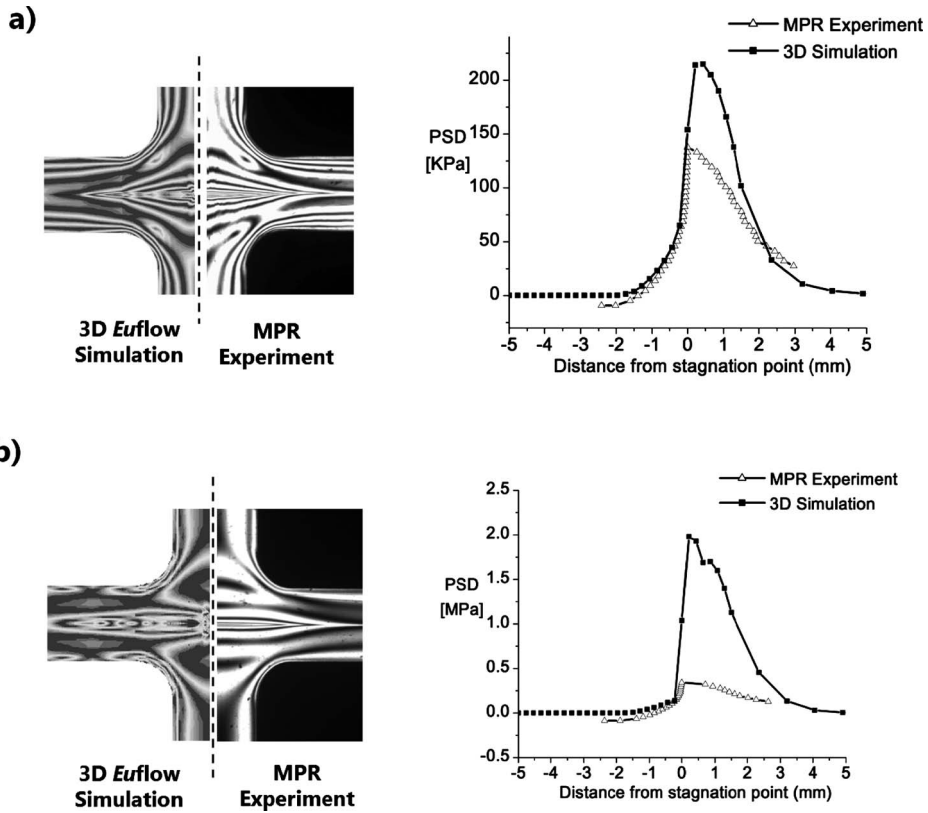


FIG. 9. The effect of cross-slot depth. Cross-slot 3D *EUFLOW* simulations and experimental MPR PSD contours and corresponding center-line PSD for (a) 7 mm depth slit ($\bar{v}=0.45$ mm s $^{-1}$, $\dot{\gamma}_w \sim 2.06$ s $^{-1}$, $\bar{Wi}=8.4$, and $Wi_m=57.2$) and (b) 1.5 mm depth slit ($\bar{v}=2.4$ mm s $^{-1}$, $\dot{\gamma}_w \sim 11.2$ s $^{-1}$, $\bar{Wi}=45.9$, and $Wi_m=310.8$).

~ 24.0 s $^{-1}$, $\bar{Wi}=98.4$, and $Wi_m=666$. A *EUFLOW* simulation was performed and the results compared in Fig. 10(a), with a very good agreement found between simulation and experiment for both pressure drop and PSD profiles. A similar comparison was undertaken for the cross-slot, with MPR experimental conditions using $\bar{v}=2.09$ mm s $^{-1}$, giving $\dot{\gamma}_w \sim 9.6$ s $^{-1}$, $\bar{Wi}=39.4$, and $Wi_m=266.4$. For this case, there is limited cusping seen in the experiment when a steady state is reached in comparison to the PS2 material, similar to that observed previously for these materials in the cross-slot [Hassell and Mackley (2009)]. The corresponding comparison to a *EUFLOW* simulation is displayed in Fig. 10(b) and illustrates the very good match achieved between simulation and experiment. This demonstrates the ability of the code to simulate complex flows in this geometry; however, its limitations are clear when studying the more challenging polydisperse polymer, PS2,

TABLE III. Table of material molecular weights for monodisperse polystyrene, DOW1568, determined using GPC.

Label	M_w (g/mol)	M_n (g/mol)	M_w/M_n
DOW1568	118 300	105 000	1.128

TABLE IV. Relaxation time spectrum and the corresponding non-linear constitutive parameters of the multi-mode Rolie-Poly model for DOW1568 at 180 °C.

DOW1568			
Mode No.	g_i (Pa)	τ_i (s)	τ_{Ri} (s)
1	4.320×10^5	0.000 10	
2	8.219×10^4	0.000 84	
3	8.183×10^4	0.006 86	
4	7.280×10^4	0.056 23	0.10
5	3.159×10^3	0.460 80	0.87

which provides a more robust test of the constitutive equation and numerical solver.

IV. CONCLUSIONS

This paper has shown that it is possible to simulate 3D viscoelastic flow of a commercial linear polymer melt within certain complex flows using a fully 3D time depen-

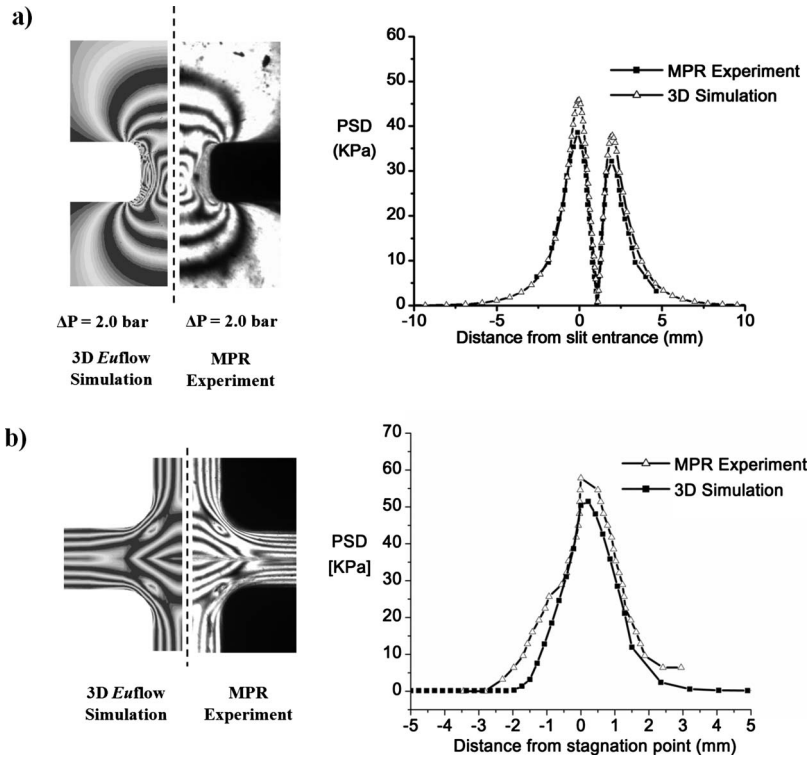


FIG. 10. Matching experimental MPR flow of monodisperse polystyrene with 3D *EUFLOW* simulations. (a) 10 mm depth slit flow PSD contours, center-line PSD, and overall pressure drop comparison of 3D *EUFLOW* to experimental MPR flow, $\bar{v}=0.78$ mm s⁻¹, $\dot{\gamma}_w \sim 24.0$ s⁻¹, $\bar{Wi}=98.4$, and $Wi_m=666$. (b) 10 mm depth cross-slot flow PSD contours and corresponding center line PSD comparison of 3D *EUFLOW* simulations to experimental MPR $\bar{v}=2.09$ mm s⁻¹, $\dot{\gamma}_w \sim 9.6$ s⁻¹, $\bar{Wi}=39.4$, and $Wi_m=266.4$.

dent solution of the Rolie-Poly model with results validated by experiment. Both linear and non-linear viscoelastic characterizations of the polystyrene melt were employed in order to describe its flow behavior. In this paper, a single set of parameters, fitted to the rheological data, was used. There is, however, not a unique set of material parameters for this material and different fitting procedures can yield different data parameter sets which in turn can be anticipated to give slightly different flow simulation predictions, especially when the distributions of stretch times for this polydisperse sample are considered.

An important finding of this paper is the confirmation that a 10 mm depth slit approximates to that of a 2D flow. [Clemeur *et al.* \(2004\)](#) have previously shown this numerically and the results presented in Fig. 5 of this paper show for a 10 mm depth slit that there is a good match between 2D and 3D simulations and both match experimental MPR results with good accuracy.

In order to match any simulation with experimental MPR data, visual PSDs have been presented together with center-line contour plots. In addition, the overall pressure drops have been compared and the data presented, for example, in Fig. 5, gives an impressive match between simulation and experiment. The effect of slit depth has also been explored and here the fit between experiment and simulation is reasonably satisfactory indicating that the 3D *EUFLOW* solver can handle genuinely 3D flow as, for example, in Fig. 7(b), the slit width and depth are nearly the same.

For the case of the cross-slot, the match between simulation and experiment is less impressive. The high strain created in the center of the cross-slot field apparently creates challenging regions for both rheological characterization and simulation. At this stage, it is not possible to say whether the lack of fit is through a failing in the rheological model, grid size, or the numerical simulation.

Overall, the paper demonstrates the effectiveness of the MPR to generate high precision experimental data and the effectiveness of the multi-mode Rolie-Poly constitutive equation and 3D *EUFLOW* simulations to model the flow for both slit and cross-slot geometries. The results indicate that both the rheological characterization and simulations can now be used with confidence for even more complex processing situations.

ACKNOWLEDGMENTS

This work was supported by the EPSRC (U.K.) under the “Microscale Polymer Processing Consortium for Macromolecular Engineering: Toolbox Development and Application” Grant (Grants No. GR/T11821/01 and No. GR/T11807/01). The authors wish to acknowledge BASF SE and DOW Chemicals for supplying the polymer material, Dr. Lian Hutchings for the GPC data, and Dr. S. Butler for MPR technical assistance.

References

- Alves, M. A., F. T. Pinho, and P. J. Oliveira, “Viscoelastic flow in a 3D square/square contraction: Visualizations and simulations,” *J. Rheol.* **52**, 1347–1368 (2008).
- Auhl, D., J. Ramirez, A. E. Likhtman, P. Chambon, and C. Fernyhough, “Linear and nonlinear shear flow behaviour of monodisperse polyisoprene melts with a large range of molecular weights,” *J. Rheol.* **52**, 801–835 (2008).
- Baaijens, F. P. T., “Mixed finite element methods for viscoelastic flow analysis: A review,” *J. Non-Newtonian Fluid Mech.* **79**, 361–385 (1998).
- Binding, D. M., P. M. Phillips, and T. N. Phillips, “Contraction/expansion flows: The pressure drop and related issues,” *J. Non-Newtonian Fluid Mech.* **137**, 31–38 (2006).

- Bogaerds, A. C. B., W. M. H. Verbeeten, G. W. M. Peters, and F. P. T. Baaijens, "3D viscoelastic analysis of a polymer solution in a complex flow," *Comput. Methods Appl. Mech. Eng.* **180**, 413–430 (1999).
- Clemeur, N., R. P. G. Rutgers, and B. Debbaut, "Numerical evaluation of three dimensional effects in planar flow birefringence," *J. Non-Newtonian Fluid Mech.* **123**, 105–120 (2004).
- Collis, M. W., A. K. Lele, M. R. Mackley, R. S. Graham, D. J. Groves, A. E. Likhtman, T. M. Nicholson, O. G. Harlen, T. C. B. McLeish, L. Hutchings, C. M. Fernyhough, and R. N. Young, "Constriction flows of monodisperse linear entangled polymers: Multiscale modelling and flow visualization," *J. Rheol.* **49**, 501–522 (2005).
- Collis, M. W., and M. R. Mackley, "The melt processing of monodisperse and polydisperse polystyrene melts within a slit entry and exit flow," *J. Non-Newtonian Fluid Mech.* **128**, 29–41 (2005).
- Coventry, K. D., and M. R. Mackley, "Cross-slot extensional flow birefringence observations of polymer melts using a multi-pass rheometer," *J. Rheol.* **52**, 401–415 (2008).
- Crowley, D. G., F. C. Frank, M. R. Mackley, and R. C. Stephenson, "Localised flow birefringence of polyethylene oxide solutions in a four roll mill," *J. Polym. Sci. A* **2**(14), 1111–1119 (1976).
- Fan, Y. R., R. I. Tanner, and N. J. Phan-Thien, "Galerkin/least-square finite-element methods for steady viscoelastic flows," *J. Non-Newtonian Fluid Mech.* **84**, 233–256 (1999).
- Ferry, J. D., *Viscoelastic Properties of Polymers* (Wiley, New York, 1980).
- Friedrich, C., W. Waizenegger, and H. H. Winter, "Relaxation patterns of long, linear, flexible, monodisperse polymers: BSW spectrum revisited," *Rheol. Acta* **47**, 909–916 (2008).
- Fuller, G. G., *Optical Rheometry of Complex Fluids* (Oxford University Press, New York, 1995).
- Graham, R. S., A. E. Likhtman, S. T. Milner, and T. C. B. McLeish, "Microscopic theory of linear entangled polymer chains under rapid deformation including chain stretch and convective constraint release," *J. Rheol.* **47**, 1171–1200 (2003).
- Han, C. D., and L. H. Dexler, "Studies of converging flows of viscoelastic polymeric melts. I. Stress birefringence measurements in the entrance region of a sharp-edged slit die," *J. Appl. Polym. Sci.* **17**, 2329–2354 (1973).
- Harlen, O. G., J. M. Rallison, and P. Szabo, "A split Lagrangian-Eulerian method for simulating transient viscoelastic flows," *J. Non-Newtonian Fluid Mech.* **60**, 81–104 (1995).
- Hassell, D. G., D. Auhl, T. C. B. McLeish, and M. R. Mackley, "The effect of viscoelasticity on stress fields within polyethylene melt flow for a cross-slot and contraction-expansion slit geometry," *Rheol. Acta* **47**, 821–834 (2008).
- Hassell, D. G., J. Embery, T. C. B. McLeish, and M. R. Mackley, "An experimental evaluation of the formation of an instability in mono and polydisperse polystyrenes," *J. Non-Newtonian Fluid Mech.* **157**, 1–14 (2009).
- Hassell, D. G., and M. R. Mackley, "An experimental evaluation of the behaviour of mono and polydisperse polystyrenes in cross-slot flow," *Rheol. Acta* **48**, 543–550 (2009).
- Hulsen, M. A., E. A. J. F. Peters, and B. H. A. A. van den Brule, "A new approach to the deformation fields method for solving complex flows using integral constitutive equations," *J. Non-Newtonian Fluid Mech.* **98**, 201–221 (2001).
- Inkson, N. J., T. C. B. McLeish, O. G. Harlen, and D. J. Groves, "Predicting low density polyethylene melt rheology in elongational and shear flows with "pom-pom" constitutive equations," *J. Rheol.* **43**, 873–896 (1999).
- Inkson, N. J., T. N. Phillips, and R. G. M. van Os, "Numerical simulation of flow past a cylinder using models of XPP type," *J. Non-Newtonian Fluid Mech.* **156**, 7–20 (2009).
- Keunings, R., *Simulation of Viscoelastic Flow*, Computer Modeling for Polymer Processing, edited by C. L. Tucker (Hanser, Munich, 1989), pp. 404–469.
- Lee, K., M. R. Mackley, T. C. B. McLeish, T. M. Nicholson, and O. Harlen, "Experimental observation and numerical simulation of transient stress fringes within flowing molten polyethylene," *J. Rheol.* **45**, 1261–1277 (2001).
- Likhtman, A. E., and R. S. Graham, "Simple constitutive equation for linear polymer melts derived from molecular theory: Rolie-Poly equation," *J. Non-Newtonian Fluid Mech.* **114**, 1–12 (2003).
- Luo, X. L., and E. Mitsoulis, "An efficient algorithm for strain history tracking in finite element computations of non-Newtonian fluids with integral constitutive equations," *Int. J. Numer. Methods Fluids* **11**, 1015–1031

- (1990).
- Mackley, M. R., R. T. J. Marshall, and J. B. A. F. Smeulders, "The multi-pass rheometer," *J. Rheol.* **39**, 1293–1309 (1995).
- Mackley, M. R., R. T. J. Marshall, J. B. A. F. Smeulders, and F. D. Zhao, "The rheological characterization of polymeric and colloidal fluids," *Chem. Eng. Sci.* **49**, 2551–2565 (1994).
- Macosko, C. W., *Rheology, Principles, Measurements and Applications* (Wiley-VCH, New York, 1994).
- McLeish, T. C. B., and R. G. Larson, "Molecular constitutive equations for a class of branched polymers: The pom-pom polymer," *J. Rheol.* **42**, 81–110 (1998).
- Oliveira, P. J., F. T. Pinho, and G. A. Pinto, "Numerical simulation of non-linear elastic flows with a general collocated finite-volume method," *J. Non-Newtonian Fluid Mech.* **79**, 1–43 (1998).
- Phan-Thien, N., and R. I. Tanner, "A new constitutive equation derived from network theory," *J. Non-Newtonian Fluid Mech.* **2**, 353–365 (1977).
- Phillips, T. N., and R. G. Owens, *Computational Rheology* (Imperial College Press, London, U.K., 2002).
- Puangkird, B., F. Belblidia, M. F. Webster, "Numerical simulation of viscoelastic fluids in cross-slot devices," *J. Non-Newtonian Fluid Mech.* **162**, 1–20 (2009).
- Rasmussen, H. K., "Lagrangian viscoelastic flow computations using a generalized molecular stress function model," *J. Non-Newtonian Fluid Mech.* **106**, 107–120 (2002).
- Saad, Y., *Iterative Methods for Sparse Linear Systems*, 2nd ed. (SIAM, Philadelphia, PA, 2003).
- Soulages, J., T. Schweizer, D. C. Venerus, M. Kroger, and H. C. Ottinger, "Lubricated cross-slot flow of a low density polyethylene melt," *J. Non-Newtonian Fluid Mech.* **154**, 52–64 (2008).
- Tenchev, R., O. Harlen, P. K. Jimack, and M. A. Walkley, in *Finite Element Modelling of Two- and Three-Dimensional Viscoelastic Polymer Flows*, Trends in Engineering Computational Technology, edited by M. Papadarakakis and B. H. V. Topping (Saxe-Coburg Publications, Stirling, U.K., 2008), pp. 81–101.
- Verbeeten, W. M. H., G. W. M. Peters, and F. P. T. Baaijens, "Viscoelastic analysis of complex polymer melt flows using the eXtended Pom-Pom model," *J. Non-Newtonian Fluid Mech.* **108**, 301–326 (2002).
- Wagner, M. H., and H. M. Laun, "Non-linear shear creep and constrained elastic recovery of a LDPE melt," *Rheol. Acta* **17**, 138–148 (1978).
- Wagner, M. H., V. H. Rolon-Garrido, J. K. Nielsen, H. K. Rasmussen, and O. Hassager, "A constitutive analysis of transient and steady-state elongational viscosities of bidisperse polystyrene blends," *J. Rheol.* **52**, 67–86 (2008).
- Walkley, M. A., P. H. Gaskell, P. K. Jimack, M. A. Kelmanson, and J. L. Summers, "Finite element simulation of three-dimensional free-surface flow problems," *J. Sci. Comput.* **24**, 147–162 (2005).
- Wapperom, P., and M. F. Webster, "Simulation for viscoelastic flow by a finite volume/element method," *Comput. Methods Appl. Mech. Eng.* **180**, 281–304 (1999).
- Yu, C. C., and J. C. Heinrich, "Petrov–Galerkin method for multidimensional, time-dependent, convective-diffusion equations," *Int. J. Numer. Methods Eng.* **24**, 2201–2215 (1987).